CMS Physics Analysis Summary

Contact: cms-pag-conveners-bphysics@cern.ch 2013/04/18

Measurement of Angular Correlations Between Beauty Jets Produced in pp Collisions at 7 TeV

The CMS Collaboration

Abstract

A measurement of the angular correlations between beauty jets produced in pp collisions at a center-of-mass energy of 7 TeV at LHC is presented. A heavy-flavor enriched event sample is selected by a low-transverse-momentum single-muon trigger. Hadronic jets are identified as beauty jets by the presence of nearby high impact parameter tracks. The measured differential di-beauty jet production cross sections, $\frac{d\sigma}{d\Delta\phi}$ and $\frac{d\sigma}{d\Delta R}$, are obtained from a sample whose integrated luminosity corresponds to $3\,\mathrm{pb}^{-1}$. The visible kinematic phase-space is defined by the requirement of two b-tagged jets with $p_T > 30$ GeV and $|\eta| < 2.4$, with an angular separation of $\Delta R > 0.6$ between them, one of the jets has a muon within its decay products with $p_T > 8$ GeV and $|\eta| < 2.1$. The results obtained in data are compared with predictions based on perturbative QCD calculations.

1 Introduction

Beauty quarks are pair-produced through strong interactions in pp collisions at the CERN Large Hadron Collider (LHC). Studying the hadroproduction of beauty quark pairs $b\bar{b}$ allows for a meaningful test of perturbative Quantum Chromodynamics. At leading order (LO), i.e. in $2 \to 2$ parton interactions, conservation of momentum causes the b and $\bar{\text{b}}$ quarks to be emitted with a back-to-back topology. Higher order $2 \to 2 + n$ $(n \geq 1)$ subprocesses having additional partons (mostly gluons) emitted give rise to final state topologies with smaller opening angles. Therefore, measurements of $b\bar{b}$ angular correlations supply knowledge about the underlying production subprocesses and allow for an insightful test of perturbative Quantum Chromodynamics.

The LO mechanism of $b\bar{b}$ production is known as flavor creation where a $b\bar{b}$ is produced back-to-back with a large opening angle between the two b quarks [1, 2]. The primary mechanisms of NLO $b\bar{b}$ production are gluon splitting and flavor excitation. In gluon splitting a gluon splits into a $b\bar{b}$ giving rise to two roughly co-linear b quarks with a small opening angle between them. In flavor excitation a $b\bar{b}$ is produced within the parent proton and only one of the b quarks participates in the hard interaction. Additionally, b quarks produced via NLO mechanisms have asymmetric values of transverse momentum.

In this paper angular correlations between pairs of beauty jets are studied at $\sqrt{s} = 7\,\text{TeV}$ with the Compact Muon Solenoid (CMS) Detector. Details regarding the CMS Detector are given in Ref. [3]. The subdetectors used in this study are the tracker, calorimeters, and muon detector. The tracking detector and calorimeters are located within the superconducting solenoid, which provides a 3.8 T axial magnetic field; while the muon detector is located exterior to the solenoid, interlaced with the magnetic return yokes. The tracker consists of a silicon pixel and silicon strip tracker and is responsible for detecting charged particles within the pseudorapidity $\eta = -\ln[\tan(\theta/2)]$ range of $|\eta| < 2.5$, θ being the polar angle. The pixel tracker is comprised of three barrel layers and two endcap disks on each end of the barrel layers. The strip tracker has ten such barrel layers encapsulated by 12 endcap disks. The barrel and endcap calorimeters cover a pseudorapidity range of $|\eta| < 3.0$, and consist of a $PbWO_4$ crystal electromagnetic calorimeter and a brass/scintillator hadron calorimeter. Towers projected radially outward from the proton-proton interaction region are made from groups of electromagnetic and hadronic calorimeter cells for trigger purposes and to allow for jet reconstruction. The muon detector covers the pseudorapidity range $|\eta| < 2.4$ and is comprised of a series of drift tubes, cathode strip chambers, and resistive plate chambers.

Measurements of di-beauty jet production are presented as a function of the difference in azimuthal angle between two b-tagged jets, $\Delta\phi$, and the combined separation variable $\Delta R = \sqrt{\Delta\phi^2 + \Delta\eta^2}$ where $\Delta\eta$ is the difference in pseudorapidity between the jets. These angular correlation variables are hence forth referred to as ΔA, where the jet axis approximates the flight direction of the original b quark.

The differential $B\overline{B}$ production cross sections with respect to ΔA between two B hadron secondary decay vertices was previously presented in Ref. [4]. The present work seeks to measure the differential di-beauty jet production cross section with a different approach, which improves upon the measurement of the absolute normalization. Additionally, the phase-space covered in Ref. [4] differs to what will be presented herein.

2 Data Samples

2.1 Simulation

A muon-enriched QCD sample was generated using the CTEQ6L1 proton parton distribution function (PDF) [5] and underlying event Tune Z2 [6] with PYTHIA v6.422 [7] for the purpose of tuning the selection, evaluating efficiencies, and to serve as a theoretical comparison to the experimental results. Two additional simulated samples were generated for further theoretical comparisons using the matrix-element generators CASCADE [8, 9], which uses un-integrated parton distribution functions, and MADGRAPH [10] which also uses the CTEQ6L1 proton PDF. The hard scattering events generated by CASCADE and MADGRAPH are passed to PYTHIA for parton shower and hadronization.

2.2 Data

The data used in this analysis corresponds to an integrated luminosity of $3\,\mathrm{pb}^{-1}$ and was collected by the CMS experiment during 2010 at a centre-of-mass energy of 7 TeV. The event sample used for the cross section measurement was collected using a low-transverse-momentum single-muon trigger when the LHC was operating at low instantaneous luminosities. As such possible effects from multiple pp interactions per bunch crossing have been neglected. Only events from runs when the CMS Detector was fully functional and with stable beam conditions are used. Events from noncollision processes are rejected by requiring a primary collision vertex [11] with at least four well reconstructed tracks, lying within 2cm of the beam axis in the transverse plane, and within 24cm of the nominal interaction point along the z-axis. Additionally events with energetic noise deposits in the hadronic calorimeter are filtered out based on pulse shape, hit multiplicity and timing criteria.

An additional event sample was collected using a collection of single-jet and multijet triggers. This provides an unbiased sample for the determination of the single-muon trigger efficiency.

3 Selection of Muons and Jets

This study measures angular correlations between two hadronic jets, one of which contains a muon, originating from the hadronization and decay of b quarks. Measurements of the differential cross sections $\frac{d\sigma}{d\Delta\phi}$ and $\frac{d\sigma}{d\Delta R}$ are performed.

The trigger used to collect data enriches the heavy-flavor content of data due to the large semileptonic branching fraction of B hadrons, $\mathcal{B}_{PDG}\left(B \to \mu\nu_\mu X\right) = 0.1095^{+0.0029}_{-0.0025}$ [1].

Muons are reconstructed using the "Tight Muon Selection" [12] and must have $p_T^\mu > 8\,\mathrm{GeV}$ and $|\eta^\mu| < 2.1$. The muon kinematic requirements correspond to the efficiency plateau of the low-transverse-momentum single-muon trigger. The same kinematic requirements are applied to generated muons in the simulation. In the simulated PYTHIA sample, all observables obtained from tight muons (or the jets they are found within) are weighted with the tight muon reconstruction efficiency scale factor $SF_\mu^{reco+id} = \epsilon^{Data}_{\mu\,reco+id}/\epsilon^{MC}_{\mu\,reco+id}$ given in Ref. [12] to compensate for the measured difference between data and simulation based efficiencies.

Jets are reconstructed from "particle-flow candidates" using the infrared- and collinear-safe anti-k_T jet clustering algorithm [13, 14] with a distance parameter of 0.5. The particle-flow candidates are a collection of charged and neutral particles reconstructed with the particle-flow algorithm [15, 16]. In the simulation generator-level jets are clustered by the anti-k_T algorithm using stable generator particles (excluding neutrinos) and a distance parameter of 0.5. Recon-

structed jets found to have (lack) a tight muon with the aforementioned kinematics as one of their constituents are referred to as mu-jets (non-mu-jets). Generator-level jets are classified as mu-jets (non-mu-jets) if they have (lack) a generator-level muon with the aforementioned kinematics as one of their stable constituents. The tight or generator-level muon found within a mu-jet is referred to as the jet's associated muon.

The standard set of jet energy corrections and quality requirements are applied to all reconstructed jets in both the data and simulated samples [17]. The jet energy resolution in simulated events is corrected to what is observed in data [17] by $p_T^{jet} = p_T^{gen} + SF_{JER} \times \left(p_T^{reco} - p_T^{gen}\right)$; where p_T^{reco} is the corrected transverse momentum of the reconstructed jet, p_T^{gen} is the transverse momentum of the reconstruct jet's matched generator-level jet, and SF_{JER} is the data over simulated p_T^{jet} resolution scale factor. In the PYTHIA simulated event sample a reconstructed jet is matched to the nearest generator-level jet if the ΔR between the reconstructed and generator-level jet pair is less than 0.25. This matching is found to be more than 99% efficient for reconstructed jets passing the previous selection criteria. Both reconstructed and generator-level jets are required to have $p_T^{jet} > 30\,\text{GeV}$ and $\left|\eta^{jet}\right| < 2.4$.

In simulated samples observables obtained from reconstructed and generator-level jets found to have (lack) a $B \to \mu\nu_\mu X$ decay within their cone are weighted by a branching fraction scale factor $SF_{\mathcal{B}}^{\mu} = \frac{\mathcal{B}_{PDG}}{\mathcal{B}_{\text{PYTHIA}}} = 1.044^{+0.027}_{-0.024}$ $\left(SF_{\mathcal{B}}^{non-\mu} = \frac{1-\mathcal{B}_{PDG}}{1-\mathcal{B}_{\text{PYTHIA}}} = 0.9948^{+0.0032}_{-0.0028}\right)$. This scale factor corrects the branching fraction of semileptonic B hadron decays in PYTHIA to what has been reported in Ref. [1].

Also in simulated samples the true flavor of a generator-level jet is determined by the presence of the heaviest-flavor hadron ancestor in the hardronization chain. The true flavor, beauty, charm, and light (i.e. from gluons or light quarks, u, d, s, referred to as *guds*) of reconstructed jets in simulated samples is taken from the reconstructed jets' generator-level jet match. The flavor of a small fraction of reconstructed jets that remain unmatched is assigned as light flavor.

4 Trigger Efficiency

The determination of the single-muon trigger efficiency follows a similar procedure to that presented in Ref. [12]. Events collected by the jet triggers are used for the data-driven muon trigger efficiency determination. These events must satisfy the following criteria: 1) only one reconstructed muon per event, 2) this muon must be associated to a jet, and 3) this jet must be tagged as a beauty jet by the track counting high efficiency (TCHE) algorithm [18, 19], with a TCHE value greater than 3.3. The muon in events passing the above criteria must also be a tight muon with $|\eta^{\mu}| < 2.1$. The jet the muon is associated to must have $p_T^{jet} > 30\,\text{GeV}$.

The trigger efficiency for a given p_T^{μ} or η^{μ} bin is given as $\epsilon_{trig} = N_{matched}/N_{all}$. Here $N_{matched}$ is the number of tight muons in a p_T^{μ} or η^{μ} bin associated with a b-tagged jet and possessing a matched trigger muon object; and N_{all} is the number of tight muons in a p_T^{μ} or η^{μ} bin associated with a b-tagged jet. A tight muon's matched trigger muon object (referred to as trigger object henceforth) is the nearest, by ΔR, trigger object if the ΔR between the tight muon and the trigger object is less than 0.5.

The overall efficiency of the single-muon trigger for tight muons with $p_T^{\mu} > 8$ GeV, $|\eta^{\mu}| < 2.1$, and found within b-tagged jets with $p_T^{jet} > 30$ GeV, was determined to be $85.5 \pm 1.1\,(\text{stat.})^{+3.9}_{-1.5}\,(\text{syst.})\%$; with the systematic uncertainties being described in Section 7. Figure 1 presents the trigger efficiency with respect to the muon kinematic observables. It is observed that the single-muon

trigger efficiency reaches a plateau for $p_T^\mu > 8\,\text{GeV}$. For muons above this p_T^μ threshold there exists some variation with respect to η^μ, which is accounted for in Section 5.1.

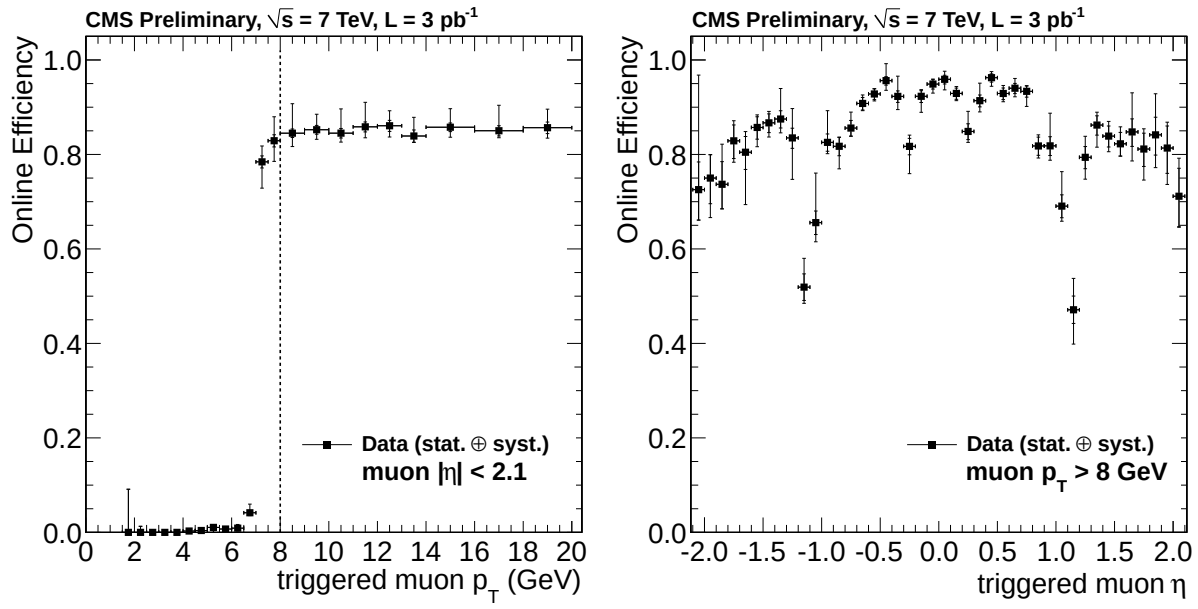

Figure 1: Left (Right): Efficiency of the online single-muon trigger used in the analysis with respect to p_T^μ for muons with $|\eta^\mu| < 2.1$ (η^μ for muons with $p_T^\mu > 8\,\text{GeV}$). Inner error bars are statistical while outer error bars are statistical and systematic added in quadrature. The vertical line on the left plot indicates the trigger muon p_T^μ threshold required for an event to be considered at further stages of selection.

5 Offline Selection

5.1 Preselection

Events selected by the single-muon trigger must have at least one reconstructed tight muon, that have a matched trigger object *and* is associated to a jet, to be considered further. However, PYTHIA events do not use the simulated trigger information and are instead weighted by $\epsilon^{Data}_{trigger}(\eta^\mu)$; where η^μ is taken from the highest p_T^μ tight muon $\left(p_T^\mu > 8\text{ GeV}\right)$ associated to a jet. The selection efficiency, Section 5.3, taken from the PYTHIA sample thus accounts for the variations observed in the single-muon trigger efficiency in data as a function of η^μ.

An event is then preselected if it has: 1) at least one mu-jet having an associated tight muon, which passes the muon kinematic cuts and has a matched single-muon trigger object and 2) at least one non-mu-jet, which by definition does not have an associated tight muon passing the muon kinematic cuts. Note that the trigger matching requirement in the first criterion is dropped for simulated PYTHIA events in favor of the data trigger efficiency weighting outlined above. Additionally, the highest TCHE mu-jet and the highest track counting high purity (TCHP) non-mu-jet are required to have $\Delta R > 0.6$. This prevents selection of poorly reconstructed and/or misidentified jet pairs that survive the jet quality requirements in Section 5.2.

5.2 B-Tagging

Jets arising from the hadronization and decay of b quarks, referred to as beauty jets, are identified by the Track Counting algorithm [18, 19]. In each event the highest TCHE mu-jet is paired

with the highest TCHP non-mu-jet to form a dijet object. The event is finally selected if the mu-jet and the non-mu-jet have TCHE > 3.3 and TCHP > 3.41, respectively. These selection criteria represent the medium ("M") and tight ("T") working points (WP), respectively referred to as TCHEM and TCHPT, for the b-tagging algorithms given in Refs. [18, 19]. The TCHEM and TCHPT WP respectively ensure a light flavor (i.e. *guds*) misidentification probability of 1% and 0.1%. Additionally, if two or more mu-jets (non-mu-jets) pass THCEM (TCHPT) requirement the event is vetoed. The fraction of events vetoed in this way is approximately 0.7% and taken as negligible.

Data-driven b-tagging scale factors for beauty, charm, and light jets, respectively SF_b, SF_c, and SF_l, are defined as the ratio of the tagging efficiency in data to that in simulation [18, 19], i.e $SF_i\left(p_T^{jet}\right) = \epsilon_i^{Data}\left(p_T^{jet}\right)/\epsilon_i^{MC}\left(p_T^{jet}\right)$ for $i = b$, c, or l. These scale factor functions are used to randomly degrade (upgrade) tagged (untagged) jets in the simulated sample. This modification is done jet-by-jet; it serves to alter the definition of a tagged jet in the PYTHIA sample to match what is observed in data.

5.3 Efficiency

The overall selection efficiency ϵ_{Sel}, online plus offline, is determined with respect to ΔA, using the simulated PYTHIA event sample (with all previously described weighting and scale factors applied), using the generator-level true beauty jet distributions and the finally selected, reconstructed, true flavor beauty jet distributions. The generator-level true beauty jets are required to have $p_T^{jet} > 30$ GeV and $\left|\eta^{jet}\right| < 2.4$. One, and only one, of these generator-level true beauty jets must have a generator-level muon with $p_T^{\mu} > 8$ GeV and $|\eta^{\mu}| < 2.1$ used in the clustering algorithm. This generator-level true beauty jet pair must also have a $\Delta R > 0.6$.

The finite jet energy resolution may allow a reconstructed beauty jet with $p_T^{reco} > 30$ GeV to be matched with a generator level beauty jet with $p_T^{gen} < 30$ GeV. This possibility was investigated by studying $\delta p_T = p_T^{reco} - p_T^{gen}$ in bins of p_T^{gen}. In each bin it was found that $\delta p_T \approx 1$ GeV. However, when considering the root-mean-square of δp_T it was observed that δp_T is consistent with zero for all bins of p_T^{gen}; as such this finite jet energy resolution matching affect is taken as negligible.

Figure 2 shows the overall selection efficiency differentially with respect to ΔA. The overall selection efficiency was found to be 17% with negligible statistical uncertainty. Systematic uncertainties associated to the selection efficiencies due to possible differences between simulation and data are discussed in Section 7.

The difference $\Delta A_{Reco} - \Delta A_{Gen}$ between finally selected true flavor beauty jet pairs and their matched generator-level true beauty jets was studied in the PYTHIA sample. The root-mean-square of this difference is taken as the angular resolution on the ΔA observables and found to be ≈ 0.03. These same jet pairs were also used to study the detector response matrix for the ΔA observables (not shown) which was observed to be strongly diagonal with off diagonal elements an order of magnitude smaller than their main diagonal counterparts. The bin width in ΔA was optimized from these resolution and detector response studies, and is taken approximately an order of magnitude larger than the ΔA resolution; as a result unfolding considerations are neglected in this study.

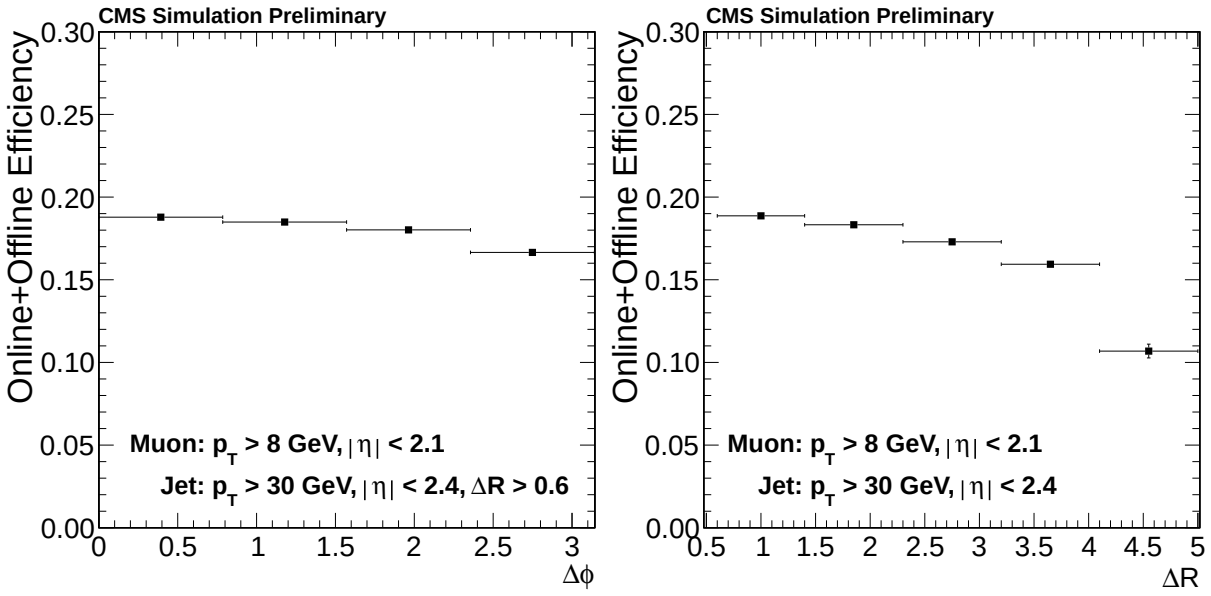

Figure 2: Total selection efficiency with respect to $\Delta\phi$ (left) and ΔR (right). The error bars depict statistical uncertainties only.

6 Signal Purity Correction

The di-beauty jet signal in data is determined by applying a bin-by-bin "purity correction" to finally selected events. Using known b-tagging efficiencies a system of four equations in four unknowns is developed and referred to as System4. The unknowns are the fractional flavor content of the jet pair in preselected events $\{bb,\, bx,\, xb,\, xx\}$ where the first (second) letter corresponds to the flavor of the mu-jet (non-mu-jet) with x representing non-beauty (i.e. charm or light). The equations break the selection into four classes of selection criterion: 1) preselection, 2) only TCHPT applied to highest TCHP non-mu-jet, 3) only TCHEM applied to highest TCHE mu-jet, 4) both TCHPT and TCHEM WP applied to their respective jets. Solving System4 for each bin of ΔA gives the purity of the final selection after the application of the appropriate efficiencies.

For the $\mathbf{S}\,\mathbf{x} = \mathbf{b}$ system represented in Eq. 1, $\mathbf{S}$, $\mathbf{x}$, and $\mathbf{b}$ are respectively referred to as the efficiency matrix, flavor vector, and yields vector. Thus, System4 is given in matrix form as:

$$\begin{bmatrix} 1 & 1 & 1 & 1 \\ \gamma_{bb}\,\epsilon_b^{TCHPT} & \gamma_{bx}\,\epsilon_x^{TCHPT} & \gamma_{xb}\,\epsilon_b^{TCHPT} & \gamma_{xx}\,\epsilon_x^{TCHPT} \\ \alpha_{bb}\,\epsilon_b^{TCHEM} & \alpha_{bx}\,\epsilon_b^{TCHEM} & \alpha_{xb}\,\epsilon_x^{TCHEM} & \alpha_{xx}\,\epsilon_x^{TCHEM} \\ \beta_{bb}\,\epsilon_{bb} & \beta_{bx}\,\epsilon_{bx} & \beta_{xb}\,\epsilon_{xb} & \beta_{xx}\,\epsilon_{xx} \end{bmatrix} \begin{bmatrix} f_{bb} \\ f_{bx} \\ f_{xb} \\ f_{xx} \end{bmatrix} = \begin{bmatrix} 1 \\ f^{TCHPT} \\ f^{TCHEM} \\ f^{Both} \end{bmatrix} \quad (1)$$

where f_{ij} are the fractional flavor content of the jet pair in preselected events ($i,\, j = b$ or x), the first (second) letter is the flavor of the mu-jet (non-mu-jet). The set $\{f^{TCHPT},\, f^{TCHEM},\, f^{Both}\}$ represents the fraction of preselected events passing each of the above selection criterion. The b-tagging efficiencies are taken from the simulated PYTHIA sample and weighted to data with the b-tagging scale factors, as described above. The b-tagging efficiencies for the TCHEM and TCHPT WPs are respectively ϵ_i^{TCHEM} and ϵ_j^{TCHPT}. Here the efficiency to tag a non-beauty jet is calculated for both the TCHEM and TCHPT WPs via $\epsilon_x = \left(n_x^{tag}\right) / \left(n_x^{tag} + n_x^{untag}\right) =$

$\left(n_c^{all}\,\epsilon_c + n_l^{all}\,\epsilon_l\right) / \left(n_c^{all} + n_l^{all}\right)$ where n_c^{all} and n_l^{all} are respectively the total number of charm and light jets in the simulated PYTHIA sample. That is the fractions of light and charm jets are taken from the simulation with appropriate systematics discussed later. The charm tagging efficiency is given as ϵ_c. The light tagging efficiency is given as ϵ_l. The product of the b-tagging efficiencies is given as $\epsilon_{ij} = \epsilon_i^{TCHEM}\,\epsilon_j^{TCHPT}$. The factors $\kappa_{ij} = \left\{\left\{\alpha_{ij}\right\},\left\{\beta_{ij}\right\},\left\{\gamma_{ij}\right\}\right\}$ are taken from the simulated PYTHIA sample as the ratios of the dijet efficiency to the single-jet b-tagging efficiency for their respective selection criterion, defined as:

$$\alpha_{ij} = \frac{\epsilon_{ij}^{Mu\,Tag}}{\epsilon_i^{TCHEM}},\ \beta_{ij} = \frac{\epsilon_{ij}^{Both\,Tag}}{\epsilon_i^{TCHEM}\,\epsilon_j^{TCHPT}},\ \gamma_{ij} = \frac{\epsilon_{ij}^{Non\,Mu\,Tag}}{\epsilon_j^{TCHPT}} \tag{2}$$

where $\epsilon_{ij}^{Mu\,Tag}$, $\epsilon_{ij}^{Non\,Mu\,Tag}$, and $\epsilon_{ij}^{Both\,Tag}$ are the efficiencies to tag the ij dijet object. They are defined as the number of ij dijet objects tagged to the total number of ij dijet objects, i.e. $\epsilon_{ij}^{Mu\,Tag} = N_{ij}^{Tag} / \left(N_{ij}^{Tag} + N_{ij}^{Untag}\right)$. Once f_{ij} is known, the purity of the ij dijet case can be calculated as $P_{ij} = \left(\beta_{ij}\,\epsilon_{ij}\right)\,\left(f_{ij}/f^{Both}\right)$.

A toy MC approach is used to determine the elements of the flavor vector and their uncertainties. One-hundred-thousand pseudo-experiments are performed for each bin of ΔA. For each pseudo-experiment the elements of the yields vector and the efficiency matrix are randomly varied by their statistical uncertainties (i.e. the element in the mn position of **S** is varied by its uncertainty and similarly for the elements of **b**), assuming that these parameters have a Gaussian distribution. System4 is then solved using the nonnegative least-squares algorithm of Lawson & Hanson [20] for each pseudo-experiment. This algorithm ensures that the calculated elements of the flavor vector are positive definite.

From these pseudo-experiments distributions of f_{ij} and P_{ij} are formed. Each distribution is then fit with a Gaussian; the mean (standard deviation) of this Gaussian is then assigned to the value (statistical uncertainty) of f_{ij} or P_{ij}.

A MC closure test is performed with the toy MC method described above. The simulated PYTHIA event sample is split into two statistically independent datasets. One sample is treated as simulation and used to construct the efficiency matrix. The other sample is treated as pseudo-data and used to construct the yields vector. For each bin of ΔA the elements of the flavor vector are compared to their corresponding true values obtained from the pseudo-data sample. Two MC closure tests are performed. In the first the κ_{ij} factors are calculated using Eq. 2. For the second the κ_{ij} factors are set to unity. Better agreement between the System4 solution and the true f_{ij} values is found when κ_{ij} factors are calculated by Eq. 2 than when κ_{ij} are set to unity. The shape of the κ_{ij} factors is taken as a systematic uncertainty.

The toy method described above is also applied to events from data. In each pseudo-experiment for the data case, System4 attempts to solve for the flavor vector in data for each bin of ΔA. The calculated selection purity corresponding to the bb flavor case obtained in data is shown in Fig. 3. The overall purity in data obtained from System4 is determined to be $P_{bb}^{Data} = 0.933 \pm 0.017\,(\text{stat.})$. While the overall true purity in the simulated sample is found to be $P_{bb}^{MC} = 0.945$ with negligible statistical uncertainty.

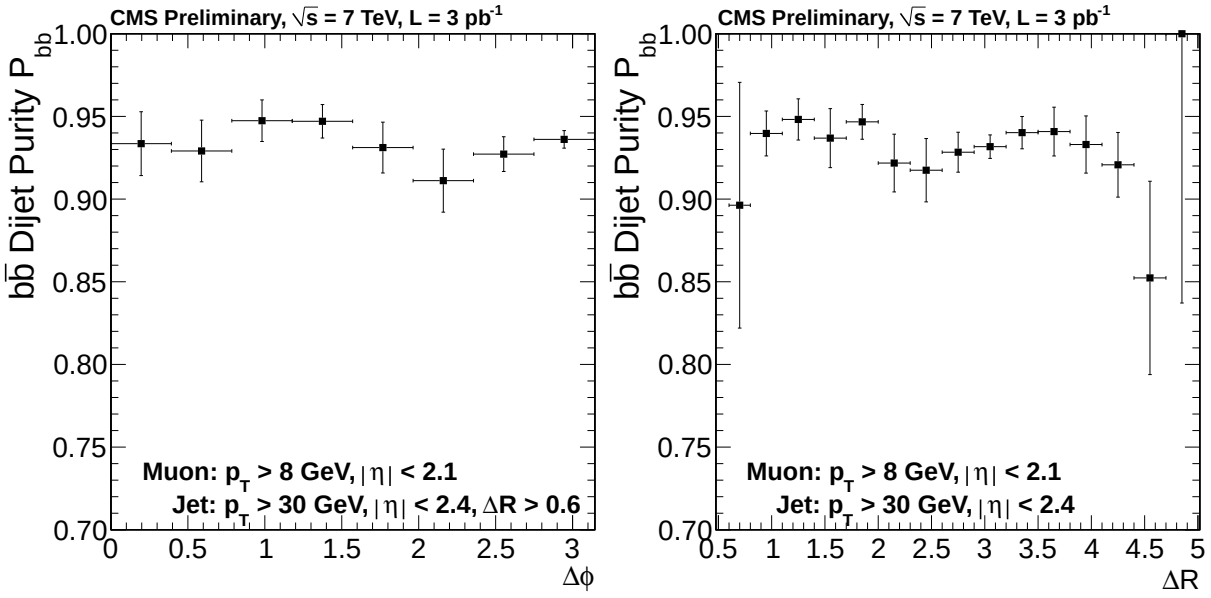

Figure 3: Left (right): Di-beauty jet signal purity of the event sample used for the cross section calculation with respect to $\Delta\phi$ (ΔR). The error bars depict statistical uncertainties only.

7 Systematic Uncertainties

A summary of all experimental systematic uncertainties considered for this analysis are given below; the affect on the total cross section $\sigma_{b\bar{b}}$ is given for each bullet. All sources of uncertainties (except for recorded integrated luminosity and trigger efficiency) are studied bin-by-bin.

Shape of Selection Efficiency: differing kinematic behavior of beauty jets between data and simulation may cause variations in the final selection efficiencies. Similarly to what was presented in Ref. [4], the nominal selection efficiency for each bin of ΔA was modified by $\epsilon'_{Sel} = \epsilon_{Sel} \times \left(1 + \frac{\delta\epsilon}{\epsilon_1}\right)$, where $\delta\epsilon = \epsilon\left(\left\langle p_T^{jet}\right\rangle_{Data}\right) - \epsilon\left(\left\langle p_T^{jet}\right\rangle_{MC}\right)$, $\epsilon_1 = \epsilon\left(\left\langle p_T^{jet}\right\rangle_{MC}\right)$, and $\left\langle p_T^{jet}\right\rangle$ is the average highest or lowest p_T^{jet} out of the jet pair in the ΔA bin of interest. This is performed for three $\left|\eta^{jet}\right|$ bins, given as $\{[0.0, 2.4], [0.0, 0.9], [0.9, 2.4]\}$, for both the highest and lowest $\left\langle p_T^{jet}\right\rangle$, six cases in total. The cross section distributions are re-computed for each new set of ϵ'_{Sel} distributions from the six separate cases; the maximum difference in each bin of ΔA between the nominal cross section and the six new cross sections is taken as the systematic uncertainty. The effect of these variations resulted in a +2.6/-0.5% change in the total cross section.

Selection Purity: possible systematic uncertainties in the selection purity are addressed by investigating: 1) poor modelling of the shapes of the κ_{ij} factors, 2) the difference $\delta_{f_{bb}} = f_{bb}^{True} - f_{bb}^{Closure}$ between the true PYTHIA f_{bb} values and the System4 solution obtained in the MC closure test for each bin of ΔA, and 3) possible differences in the relative fraction of charm and light jets in data and simulation. In the first case, System4 is solved and the cross section recomputed after varying the shapes of κ_{ij} factors. The shapes are varied by modifying the efficiencies given in the numerators of Eq. 2 in the same way that ϵ_{Sel} was modified above, with $\left\langle p_T^{jet}\right\rangle_{MC}$ and $\left\langle p_T^{jet}\right\rangle_{Data}$ taken at the appropriate selection criterion, Section 6, from the appropriate jet (mu-jet or non-mu-jet). In the second case, f_{bb}^{Data} is modified via $f'_{bb} = f_{bb}^{Data} + \delta_{f_{bb}}$. Then, f'_{bb} is

substituted into the P_{ij} equation, Section 6, and the cross section is recomputed. In the third case, when ϵ_x the value of n_c^{all} $\left(n_l^{all}\right)$ was varied up and down by a factor of two while holding n_l^{all} $\left(n_c^{all}\right)$ fixed. The cross section was then recomputed using the new ϵ_x value under each of these variations. The differences between each bin of the nominal cross section and each of these varied cross sections are added in quadrature; the effect of these variations resulted in a +3.9/-4.1% change in the total cross section.

Recorded Integrated Luminosity: currently the CMS experiment has computed the recorded integrated luminosity to a precision of 4% [21].

Muon Reconstruction Efficiency: the tight muon reconstruction efficiency scale factor $SF_{\mu}^{reco+id}$ used in the simulated PYTHIA sample is varied up and down by its uncertainties, given in Ref. [12]. The upward (downward) variation of $SF_{\mu}^{reco+id}$ results in a -1.2% (+1.2%) change in the total cross section.

Trigger Efficiency: the systematic uncertainty on the trigger efficiency presented in Section 4 is assessed using the same methodology presented in Ref. [12] by: 1) increasing the muon quality cuts beyond the standard tight muon selection, 2) increasing the b-tagging cut on the jet the trigger muon is associated with from TCHEM to TCHPT, 3) using only muons whose track determines the jet's TCHE value, and 4) with and without the b-tagging requirement under both the standard Tight Muon Selection and the increased muon selection. The upward (downward) variation of the trigger efficiency resulted in a -4.4% (+1.7%) change in the total cross section.

B-Tagging Scale Factors: the b-tagging scale factors, SF_i^{TCHEM} and SF_i^{TCHPT} (for $i = b, c, or\ l$), were varied in the same direction about their nominal values by their uncertainties when applying them jet-by-jet to upgrade (degrade) untagged (tagged) jets in the simulated sample (Section 5.2). The beauty and charm ($i = b\ or\ c$) scale factors for each algorithm are taken to be correlated with each other (i.e. SF_b^{TCHEM} is correlated with SF_c^{TCHEM}, and SF_b^{TCHPT} is correlated with SF_c^{TCHPT}), and are therefore varied simultaneously. The light scale factors for each algorithm are taken to be uncorrelated with their beauty and charm counterparts, and are therefore varied independently from their charm and beauty counterparts. The upward (downward) variation of the scale factors resulted in a -3.2% (+6.7%) change in the total cross section.

Jet Energy Scale: due to the non-linear energy response of the calorimeters, a jet energy correction must be applied to the recorded jet energy observed by the detector [17]. The transverse momentum of each jet in simulated events is varied, before applying the selection, by the uncertainty in the jet energy scale. The differential selection efficiency with respect to ΔA is recomputed in the simulation for the jet energy correction variation cases, and used to recompute the experimental cross section. The upwards (downwards) variation of the jet energy corrections resulted in a -5.6% (+9.1%) change in the total cross section.

Jet Energy Resolution: the data over simulated p_T^{jet} resolution scale factor SF_{JER} is varied by its total uncertainty given in Ref. [17] before applying the selection. The overall selection efficiency with respect to ΔA was recomputed in the simulation for the up and down variations of SF_{JER}, and used to recompute the experimental cross section. The upwards (downwards) variation of the jet energy resolution scale factor resulted in a +1.1% (+1.7%) change in the total cross section. For a conservative estimate the maximum of these variations, +1.7%, is used when calculating the total systematic uncertainty.

Fragmentation: the simulated PYTHIA sample describe in Section 2.1 was generated with the Lund symmetric fragmentation function with heavy quark endpoints modified by the Bowler

string evolution [7]. Two additional PYTHIA samples were generated using this Lund model and the Peterson/SLAC fragmentation function [7] with $\epsilon_c = 0.062$ and $\epsilon_b = 0.00406$ as given in Refs. [22] and [23]. The differences between the generator level p_T^{jet} distributions (for beauty and charm) obtained with these different fragmentation functions were used to modify the generator-level jet and reconstructed p_T^{jet} (for beauty and charm) in the simulated PYTHIA sample describe in Section 2.1, before applying the selection, via $p'_T = p_T + (f_{Lund}(p_T) - f_{Peterson}(p_T))/m$ where $f_{Lund}(p_T)$ and $f_{Peterson}(p_T)$ are respectively the values of the p_T spectrums generated with Lund and Peterson/SLAC fragmentation functions, and m is the slope of the distributions (found to be the same within statistical errors). The generator-level muon and reconstructed muon p_T were also modified in the identical fashion. The cross section was recomputed after these p_T variations and a change of +0.4% was observed in the total cross section.

PDFs: uncertainties coming from limited knowledge of the proton PDFs are assessed via the re-weighting technique described in Ref. [24]. Three PDFs were used in the re-weighting procedure, CTEQ66m, MSTW2008-nlo, and NNPDF2.0 [25–27]. Each of the PDF re-weighted selection efficiencies obtained from the simulated PYTHIA sample were found to be higher than the nominal efficiency; the cross section was recomputed for each of these new selection efficiency distributions. The maximum deviation per bin of ΔA between the nominal cross section and the re-weighted cross sections was taken as the systematic uncertainty. The effect on the total cross section was found to be -1.0%.

Table 1 shows a summary of the effect of these systematic uncertainties on the total cross section, found to be -9.8% and +13.1%. The systematic uncertainties assigned to the recorded integrated luminosity and trigger efficiency are applied as a flat value across all bins of the angular observable ΔA. The remaining systematic uncertainty sources are considered for each bin of ΔA. Table 2 shows the bin-by-bin systematic uncertainty values on the differential cross section over the range of ΔA.

8 Results

The differential cross section for the i^{th} bin of an angular observable ΔA is defined as:

$$\left(\frac{d\sigma}{d\Delta A}\right)_i = \frac{N^{Data}\, P_{bb}}{\mathcal{L}\, \Delta A_{bin}\, \epsilon_{b\bar{b}}^{Total}},$$

where N^{Data} is the number of events recorded for the i^{th} bin of ΔA measured in data, P_{bb} is the di-beauty jet signal purity for the i^{th} bin of ΔA (Fig. 3), $\mathcal{L} = 3.00 \pm 0.12$ pb^{-1} is the recorded integrated luminosity, ΔA_{bin} is the bin width in ΔA, and $\epsilon_{b\bar{b}}^{Total}$ is the overall selection efficiency for the i^{th} bin of ΔA (Fig. 2). The differential di-beauty jet production cross section distributions are given in Fig. 4; an uncertainty of -5.9% and +4.4% common to all data points due to the integrated luminosity and trigger efficiency systematic uncertainties is not shown in the figure. The bin-by-bin measured cross section values are given in Table 2 with their uncertainties; the systematic uncertainties shown in Table 2 include the common uncertainties previously mentioned.

The differential cross sections with respect to the $\Delta\phi$ and ΔR between B hadron secondary decay vertices were previously published in Ref. [4]. The lowest leading p_T^{jet} bin of this previous study matches best the final event sample shown here. The results from this leading p_T^{jet} bin of Ref. [4] and those obtained in the present work were found to agree within errors [28].

Table 1: Summary of systematic uncertainties in the total cross section. The upwards and downwards columns give the direction of the shift of the parameter of interest, where the sign of the value in these columns indicates the observed change in the total cross section. The effects of the shape variations on the total cross section are given under their own heading. The observed effect on the total cross section when changing the fragmentation parameterization and the proton PDFs are indicated under the theory headings (see text). The total systematic uncertainty is shown in the last row under the summary heading.

	Downwards	Upwards
Luminosity	+4.0%	-4.0%
$SF_{\mu}^{reco+id}$	+1.2%	-1.2%
Trigger Efficiency	+1.7%	-4.4%
$SF_i^{TCHEM}$and SF_i^{TCHPT}	6.7%	-3.2%
Jet Energy Scale	+9.1%	-5.6%
Jet Energy Resolution	+1.7%	+1.1%
	Shape Variations	
Selection Efficiency	+2.6/-0.5%	
Selection Purity	+3.9/-4.1%	
	Theory Systematics	
Fragmentation	+0.4%	
PDFs	-1.0%	
	Summary	
Total	+13.1/-9.8%	

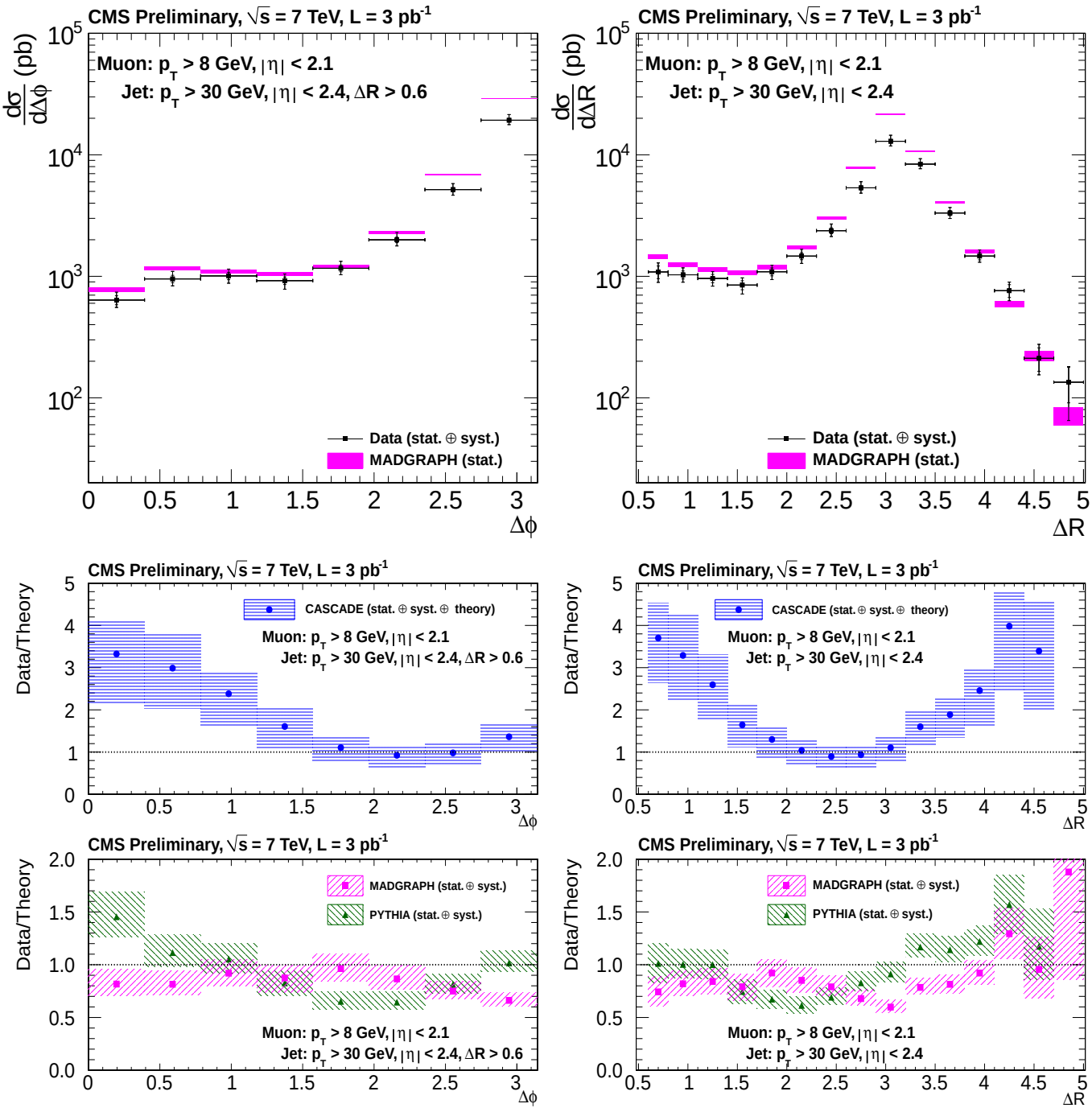

Figure 4: Differential di-beauty jet production cross section with respect to the $\Delta\phi$ (left) and ΔR (right) between two b-tagged jets obtained from data. The inner error bars represent the statistical uncertainty, while the outer error bars represent the statistical plus systematic uncertainties added in quadrature. A common uncertainty of -5.9% and +4.4% due to the integrated luminosity and trigger efficiency systematic uncertainties on the data points is not included. The theoretical comparison in the top plots was done with MADGRAPH (solid) where the band represents only statistical uncertainties. The ratio of data to theory for CASCADE, MADGRAPH, and PYTHIA is shown in the bottom plots. The band for the ratio of data to CASCADE (PYTHIA or MADGRAPH) represents the statistical, data systematic, and theoretical (statistical and data systematic) uncertainties added in quadrature.

Table 2: Summary of $d\sigma/d\Delta\phi$ and $d\sigma/d\Delta R$ differential cross sections with their statistical and systematic uncertainties given in nb.

$\Delta\phi$ Range	$\frac{d\sigma}{d\Delta\phi}$	(stat.)	(syst.)	ΔR Range	$\frac{d\sigma}{d\Delta R}$	(stat.)	(syst.)
0.000 - $\pi/8$	0.64	$\pm$0.05	$^{+0.09}_{-0.06}$	0.6 - 0.8	1.09	$\pm$0.13	$^{+0.16}_{-0.14}$
$\pi/8$ - $\pi/4$	0.95	$\pm$0.07	$^{+0.13}_{-0.10}$	0.8 - 1.1	1.03	$\pm$0.08	$^{+0.12}_{-0.11}$
$\pi/4$ - $3\pi/8$	1.01	$\pm$0.07	$^{+0.12}_{-0.11}$	1.1 - 1.4	0.96	$\pm$0.08	$^{+0.11}_{-0.11}$
$3\pi/8$ - $\pi/2$	0.92	$\pm$0.07	$^{+0.11}_{-0.12}$	1.4 - 1.7	0.85	$\pm$0.07	$^{+0.10}_{-0.11}$
$\pi/2$- $5\pi/8$	1.16	$\pm$0.08	$^{+0.15}_{-0.11}$	1.7 - 2.0	1.09	$\pm$0.08	$^{+0.12}_{-0.13}$
$5\pi/8$ - $3\pi/4$	2.00	$\pm$0.11	$^{+0.28}_{-0.19}$	2.0 - 2.3	1.47	$\pm$0.10	$^{+0.18}_{-0.16}$
$3\pi/4$ - $7\pi/8$	5.17	$\pm$0.18	$^{+0.59}_{-0.49}$	2.3 - 2.6	2.37	$\pm$0.13	$^{+0.29}_{-0.21}$
$7\pi/8$ - π	19.27	$\pm$0.39	$^{+2.14}_{-1.49}$	2.6 - 2.9	5.35	$\pm$0.20	$^{+0.63}_{-0.48}$
				2.9 - 3.2	13.93	$\pm$0.33	$^{+1.53}_{-1.05}$
				3.2 - 3.5	8.39	$\pm$0.27	$^{+0.86}_{-0.65}$
				3.5 - 3.8	3.32	$\pm$0.16	$^{+0.32}_{-0.28}$
				3.8 - 4.1	1.47	$\pm$0.10	$^{+0.15}_{-0.12}$
				4.1 - 4.4	0.76	$\pm$0.09	$^{+0.10}_{-0.10}$
				4.4 - 4.7	0.21	$\pm$0.05	$^{+0.04}_{-0.03}$
				4.7 - 5.0	0.13	$\pm$0.04	$^{+0.02}_{-0.05}$

8.1 Comparisons with Theoretical Predictions

The PYTHIA generator-level beauty jet distribution described in Section 5.3 was used to determine the ratio of data/PYTHIA theoretical cross section, Fig. 4. A similar distribution is made for CASCADE [8, 9] and MADGRAPH [10], and the ratio of data to these theoretical predictions is also shown in Fig. 4. The simulated predictions are *not* normalized to data before forming these ratios; the common systematic uncertainties arising from the trigger efficiency and recorded integrated luminosity, Sec. 7, are not considered when forming these ratios.

The uncertainty band for the data/theory plots in Fig. 4 for PYTHIA and MADGRAPH represents the statistical and systematic uncertainties added in quadrature. While the uncertainty band for the data/CASCADE plot represents the statistical, systematic, and theoretical uncertainties added in quadrature. The CASCADE theoretical uncertainties were determined by: 1) varying the renormalization scale up and down by a factor of two; 2) varying the b quark mass by 0.25 GeV about the nominal value of 4.75 GeV; 3) changing the default un-integrated parton distribution function, A0 from the CCFM set [29], to B0, also from the CCFM set [29]; and 4) changing the fragmentation model from the Lund symmetric fragmentation function with heavy quark endpoints modified by the Bowler string evolution [7] to the Peterson/SLAC model ($\epsilon_c = 0.062$ and $\epsilon_b = 0.00406$).

The absolute di-beauty jet cross sections obtained from data and simulated predictions are presented in Table 3. These estimations are done for the di-beauty jet phase-space defined by requirement of two beauty jets (found in data, or generated in simulation) produced with

$p_T^{jet} > 30$ GeV and $|\eta^{jet}| < 2.4$, with angular distance between them $\Delta R > 0.6$ and one of the jets having muon within its decay products with $p_T^{\mu} > 8$ GeV and $|\eta^{\mu}| < 2.1$.

From Fig. 4 and Tab. 3 it is seen that PYTHIA shows disagreement in the low $\Delta\phi$ region while best describing the absolute normalization. It is also seen that CASCADE has regions of disagreement in both $\Delta\phi$ and ΔR and underestimates the absolute normalization of data by 29%. Finally it is seen that MADGRAPH gives the best account of the shape of the low angular region out of the three models considered while over-estimating the absolute normalization by 29%.

Table 3: Total di-beauty jet measured and theoretical cross sections in nb for two beauty jets with $p_T^{jet} > 30$ GeV and $|\eta^{jet}| < 2.4$, with angular distance between them $\Delta R > 0.6$, and one of the jets having a muon within its decay products with $p_T^{\mu} > 8$ GeV and $|\eta^{\mu}| < 2.1$.

Data	PYTHIA	MADGRAPH	CASCADE
$12.2 \pm 0.2\,(\text{stat.})^{+1.6}_{-1.2}\,(\text{syst.})$	$13.18 \pm 0.02\,(\text{stat.})$	$17.1 \pm 0.1\,(\text{stat.})$	$9.48 \pm 0.04\,(\text{stat.})^{+1.93}_{-2.65}\,(\text{syst.})$

9 Summary

A measurement of angular correlation observables between beauty jets pair-produced in pp collisions at $\sqrt{s} = 7$ TeV within the CMS Detector is presented. The total integrated luminosity of the dataset used for this study is $3.00 \pm 0.12\,\text{pb}^{-1}$. The tagging of jets arising from the hadronization and decay of b quarks was done using the track counting algorithms TCHE and TCHP. The results given are the differential production cross sections as a function of the angular separation variables, $\Delta\phi$ and ΔR, between finally selected beauty jet candidate pairs. It was shown that out of the theoretical models considered MADGRAPH better describes the low angular region of di-beauty jet production, while PYTHIA better describes the absolute cross section.

10 Acknowledgements

We wish to congratulate our colleagues in the CERN accelerator departments for the excellent performance of the LHC machine. We thank the technical and administrative staff at CERN and other CMS institutes, and acknowledge support from: FMSR (Austria); FNRS and FWO (Belgium); CNPq, CAPES, FAPERJ, and FAPESP (Brazil); MES (Bulgaria); CERN; CAS, MoST, and NSFC (China); COLCIENCIAS (Colombia); MSES (Croatia); RPF (Cyprus); Academy of Sciences and NICPB (Estonia); Academy of Finland,ME, andHIP (Finland); CEAand CNRS/IN2P3 (France); BMBF, DFG, and HGF (Germany); GSRT (Greece); OTKA and NKTH (Hungary); DAE and DST (India); IPM (Iran); SFI (Ireland); INFN (Italy); NRF and WCU (Korea); LAS (Lithuania); CINVESTAV, CONACYT, SEP, and UASLP-FAI (Mexico); PAEC (Pakistan); SCSR (Poland); FCT (Portugal); JINR (Armenia, Belarus, Georgia, Ukraine, Uzbekistan); MST and MAE (Russia); MSTD (Serbia); MICINN and CPAN (Spain); Swiss Funding Agencies (Switzerland); NSC (Taipei); TUBITAK and TAEK (Turkey); STFC (United Kingdom); DOE and NSF (USA).

References

[1] J. Beringer et al. (Particle Data Group), "Review of Particle Physics", *Physical Review D* **86** (2012).

[2] E. Norrbin, T. Sjostrand, "Production and hadronization of heavy quarks", *Eur. Phys. J.* **17** (2000) 137, doi:10.1007/s100520000460.

[3] CMS Collaboration, "CMS physics Technical Design Report Volume I: Detector Performance and Software", *CERN-LHCC-2006-001* **CMS-TDR-008-1** (2006).

[4] CMS Collaboration, "Measurement of $B\overline{B}$ angular correlations based on secondary vertex reconstruction at $\sqrt{s}$ = 7 TeV", *JHEP03* **136** (2011).

[5] J. Pumplin, D. R. Stump, J. Huston, H. L. Lai, P. Nadolsky, W. K. Tung, "New Generation of Parton Distributions with Uncertainties from Global QCD Analysis", *JHEP07* **012** (2002) doi:10.1088/1126-6708/2002/07/012, arXiv:0201195.

[6] CMS Collaboration, "Measurement of the Underlying Event Activity at the LHC with $\sqrt{s}$ = 7 TeV and Comparison with $\sqrt{s}$ =0.9 TeV", *JHEP* **09** (2011) 109, arXiv:1107.0330.

[7] T. Sjostrand, S. Mrenna, P. Z. Skands, "PYTHIA 6.4 Physics and Manual", *JHEP* **05** (2006) 026, arXiv:0603175.

[8] H. Jung and G. Salam, "Hadronic final state predictions from CCFM: the hadron-level Monte Carlo generator CASCADE", *Eur. Phys. J.* **19** (2001) 251, arXiv:0012143.

[9] H. Jung, M. Kraemer, A. V. Lipatov, N. P. Zotov, "Investigation of beauty production and parton shower effects at LHC", *Phys. Rev. D* **85** (2012) 034035, doi:10.1103/PhysRevD.85.034035, arXiv:1111.1942.

[10] J. Alwall, M. Herquet, F. Maltoni, O. Mattelaer, T. Stelzer, "MadGraph 5: Going Beyond", *JHEP 1106* **128** (2011).

[11] CMS Collaboration, "Tracking and Primary Vertex Results in First 7 TeV Collisions", *CMS Physics Analysis Summary* **CMS-PAS-TRK-10-005** (2010).

[12] CMS Collaboration, "Performance of CMS Muon reconstruction in pp collision events at $\sqrt{s}$ = 7 TeV", *JINST* **7** (2012) doi:10.1088/1748-0221/7/10/P10002, arXiv:1206.4071.

[13] CMS Collaboration, "Jet Performance in pp Collisions at $\sqrt{s}$ = 7 TeV", *CMS Physics Analysis Summary* **CMS-PAS-JME-10-003** (2010).

[14] M. Cacciari, G. P. Salam, G. Soyez, "The anti-k_t jet clustering algorithm", *JHEP04* **063** (2008).

[15] CMS Collaboration, "Particle-Flow Event Reconstruction in CMS and Performance for Jets ,Taus and E_T^{Miss}", *CMS Physics Analysis Summary* **CMS PAS PFT-09/001** (2009).

[16] CMS Collaboration, "Commissioning of the Particle-Flow Reconstruction in Minimum-Bias and Jet Events from pp Collisions at 7 TeV", *CMS Physics Analysis Summary* **CMS-PAS-PFT-10-002** (2010).

[17] CMS Collaboration, "Determination of Jet Energy Calibration and Transverse Momentum Resolution in CMS", *J. Instrum.* **6** (2011) doi:10.1088/1748-0221/6/11/P11002, arXiv:1107.4277.

[18] CMS Collaboration, "Commissioning of b-jet identification with pp collisions at $\sqrt{s} = 7$ TeV", *CMS Physics Analysis Summary* **CMS-PAS-BTV-10-001** (2010).

[19] CMS Collaboration, "Performance of b-jet identification in CMS", *CMS Physics Analysis Summary* **CMS-PAS-BTV-11-001** (2011).

[20] Charles L. Lawson, Richard J. Hanson in *Solving Least Squares Problems*. Prentice-Hall, Inc., 1974.

[21] CMS Collaboration, "Absolute luminosity normalization", *CMS-DP-2011-002* **CERN-CMS-DP-2011-002** (2011).

[22] Grażyna Nowak on behalf of the H1 and ZEUS Collaborations, "Particle Production and Fragmentation at HERA", *Nuclear Physics B (Proc. Suppl.)* **210-211** (2011) 101–106.

[23] DELPHI Collaboration, "A study of the b-quark fragmentation function with the DELPHI detector at LEP I and an averaged distribution obtained at the Z Pole", *Eur. Phys. J. C* **71** (2011) 1557.

[24] D. Bourilkov, R. C. Group, M. R. Whalley, "LHAPDF: PDF Use from the Tevatron to the LHC", (2006). arXiv:0605240.

[25] P. M. Nadolsky, H.-L. Lai, Q.-H. Cao, J. Huston, J. Pumplin, D. Stump, W.-K. Tung, C.-P. Yuan, "Implications of CTEQ global analysis for collider observables", *Phys. Rev.* **D78** (2008) 013004, arXiv:0802.0007.

[26] A.D. Martin, W.J. Stirling, R.S. Thorne, G. Watt, "Parton distributions for the LHC", *Eur. Phys. J.* **C63** (2009) 189–285, arXiv:0901.0002.

[27] Richard D. Ball, Luigi Del Debbio, Stefano Forte, Alberto Guffanti, Jose I. Latorre, Juan Rojo, Maria Ubiali, "A first unbiased global NLO determination of parton distributions and their uncertainties", (2010). arXiv:1002.4407.

[28] CMS Collaboration, "Measurement of Angular Correlations Between Beauty Jets Produced in pp Collisions at 7 TeV, https://twiki.cern.ch/twiki/bin/view/CMSPublic/PhysicsResultsBPH10019", 2013.

[29] H. Jung, "Un-integrated PDFs in CCFM", (2004). arXiv:0411287.